Journal of Quantitative Spectroscopy & Radiative Transfer 315 (2024) 108889

Contents lists available at ScienceDirect

Journal of Quantitative Spectroscopy and Radiative Transfer

journal homepage: www.elsevier.com/locate/jqsrt

Effects of density distribution on the Stark width and shift of spectral lines in plasma

Evgeny Stambulchik *, Yitzhak Maron

Weizmann Institute of Science, 234 Herzl Street, POB 26, 7610001, Rehovot, Israel

ARTICLE INFO

Keywords:
Line shapes
Plasma broadening
Stark effect
Density distribution
Turbulence

ABSTRACT

A plasma density distribution that arises due to a finite observation volume or is inherent due to turbulence, needs to be accounted for when using spectral lines for plasma diagnostics. Such a distribution distorts line shapes in a non-trivial way and alters their intensities. In the present study, these effects are analyzed. The results are presented analytically and also tabulated for two types of the density distribution, Gaussian and log-normal, over a wide range of the distribution variance. The results are applicable to practically any type of spectral lines used for plasma density diagnostics. Provided also are considerations for choosing spectral lines to minimize uncertainties if a density distribution is expected but its extent is unknown. In addition, an approach for inferring the density distribution based on the line-shape asymmetry is suggested.

1. Introduction

Line-shape analysis is a powerful tool for plasma diagnostics [1,2]. Due to various reasons – both instrumental (finite spatial and temporal resolutions) and inherent to the physics of the plasma itself (e.g., fluctuations due to a developed turbulent motion [3,4]) – the line-shape measurements unavoidably integrate over a certain distribution of the plasma parameters. Whether such fluctuations of plasma parameters are diagnosed [4,5], assumed based on indirect considerations [3], or a priori unknown, they must be taken into consideration when line shapes are used for diagnosing plasmas.

In the absence of magnetic fields [6], the temperature T (or the electron T_e and ion T_i temperatures separately, if not equilibrated [7]) and electron density n_e are the main plasma parameters affecting line shapes through the Doppler and Stark effects. These parameters also influence the line intensities. In a previous study [8], the combined effect of the temperature fluctuations on the Doppler-broadened line shapes was investigated. When the Doppler effect contributes a minor fraction of the line broadening, it is the Stark effect due to the electric fields of the charged plasma particles that is mainly responsible for the line-shape formation [9]. For such lines, therefore, the most influential parameter is the electron density, while the temperature dependence of the Stark effect is usually weaker.

The focus of the present study is on spectral lines that have an insignificant Doppler broadening, with the major line-shape-formation factor being the plasma density through the Stark effect. Therefore, only the dependence on n_e will be explicitly maintained in the following considerations; a few remarks on accounting for the temperature dependence within the framework here developed are made in the concluding section.

A previous analysis of the effect of turbulent density fluctuations on the shapes of hydrogen Balmer lines under typical tokamak edge conditions showed a significant increase of the line widths [10]. Here, the analysis is generalized to spectral lines of practically any type. In particular, the Stark shift is taken into account, resulting in noticeable line-shape asymmetries due to the density fluctuations.

2. Line shape

The line shape emitted from a finite plasma volume δV and integrated over a finite time δt is

$$I(\omega) = \int_0^\infty I(n_e;\omega) P(n_e)\, dn_e, \tag{1}$$

where $I(n_e;\omega)$ is the line shape formed by a homogeneous plasma with the electron density n_e, and $P(n_e)$ is the probability to find n_e inside δV during δt, $\int_0^\infty P(n_e)\, dn_e = 1$. $I(n_e;\omega)$ will be further factorized into the spectrally integrated intensity $J(n_e)$ and the normalized line shape $L(n_e;\omega)$, $\int_0^\infty L(n_e;\omega)\, d\omega = 1$. Thus,

$$I(\omega) = \int_0^\infty J(n_e)\, L(n_e;\omega)\, P(n_e)\, dn_e. \tag{2}$$

This general expression does not allow for practical use, however. In order to proceed, some simplifying assumptions have to be made.

* Corresponding author.
E-mail address: Evgeny.Stambulchik@weizmann.ac.il (E. Stambulchik).

https://doi.org/10.1016/j.jqsrt.2023.108889
Received 20 November 2023; Received in revised form 21 December 2023; Accepted 21 December 2023
Available online 27 December 2023

First, the density distribution is assumed to be either Gaussian (G) or log-normal (LN) with a typical value of n_0 and a measure of variance σ_{n_e}. Introducing dimensionless quantities $\xi \equiv n_e/n_0$ and $\sigma \equiv \sigma_{n_e}/n_0$, one gets

$$P_G(\xi) = \frac{C_G(\sigma)}{\sigma\sqrt{2\pi}} \exp\left[-\frac{(\xi-1)^2}{2\sigma^2}\right] \tag{3a}$$

or

$$P_{\rm LN}(\xi) = \frac{1}{\xi\sigma\sqrt{2\pi}} \exp\left[-\frac{(\ln\xi)^2}{2\sigma^2}\right], \tag{3b}$$

respectively. The normalization correction (since $n_e \geq 0$) is

$$C_G(x) = \left[1 - \frac{1}{2}\,\mathrm{erfc}\,\frac{1}{\sqrt{2}x}\right]^{-1}. \tag{4}$$

Evidently, for $\sigma \to 0$, both distributions approach the delta function $\delta(\xi-1)$. The log-normal density probability distribution function naturally appears in the theoretical description of ideal isothermal turbulent gas (e.g., [11,12] and references therein) and, except for the far wings of the distribution, remains qualitatively correct in the refined models of turbulence, including supersonic one [13]. On the other hand, the normal (Gaussian) distribution is often a practical choice to describe a density distribution emerging due to integration over a finite space or time.

Secondly, the line shape is represented by a Lorentzian,

$$L(n_e;\omega) = \frac{1}{\pi}\frac{w(n_e)}{[\omega-\omega_0-d(n_e)]^2 + w(n_e)^2}, \tag{5}$$

where both the half-width at half-maximum (HWHM) $w(n_e)$ and the shift $d(n_e)$, relative to the unshifted spectral line position ω_0, depend on the density (it will be shown in Section 4.1, however, that the results are readily applicable to non-Lorentzian shapes). Although not universal, the Lorentzian shape is a very good approximation for a large class of spectral lines known as isolated transitions, with the main broadening mechanism well described by the electron impact approximation [9]. In fact, a large volume of line-broadening computational and experimental results for isolated lines are presented in numerous published compilations and on-line databases (e.g., [9,14–16]) as tabulated values of w[1] and d. The impact model is also a good approximation for ion broadening in low-density hydrogen plasmas [17]. Furthermore, Lorentzian emerges as the shape of the central part of hydrogen and hydrogen-like transitions with a strong central component [18]. Finally, about any line shape, unless it has a dip in the center, can be reasonably approximated in its central part by a Lorentzian.

The last assumption made is that each of $J(n_e)$, $w(n_e)$, and $d(n_e)$ is a power function of n_e in a reasonable vicinity of n_0, i.e.,

$$w(n_e) = w_0\xi^a \tag{6}$$

$$d(n_e) = d_0\xi^b \tag{7}$$

$$J(n_e) = J_0\xi^c \tag{8}$$

where the zero-indexed quantities are those at $n_e = n_0$.

Since the goal of this study is to quantify *deviations* from the "unperturbed" line shape (i.e., the line shape in the absence of density fluctuations, having HWHM of w_0 and centered at $\omega_0 + d_0$), the shifted and scaled angular frequency

$$\bar{\omega} \equiv (\omega - \omega_0 - d_0)/w_0 \tag{9}$$

and the scaled shift

$$\bar{d}_0 \equiv d_0/w_0 \tag{10}$$

are introduced, so that

$$I(\bar{\omega})/J_0 = \frac{C_G(\sigma)}{\sigma\pi\sqrt{2\pi}} \int_0^\infty d\xi \frac{\xi^{a+c}\exp\left[-\frac{(\xi-1)^2}{2\sigma^2}\right]}{\left[\bar{\omega}+\bar{d}_0(1-\xi^b)\right]^2 + \xi^{2a}} \tag{11a}$$

and

$$I(\bar{\omega})/J_0 = \frac{1}{\sigma\pi\sqrt{2\pi}} \int_0^\infty d\xi \frac{\xi^{a+c-1}\exp\left[-\frac{(\ln\xi)^2}{2\sigma^2}\right]}{\left[\bar{\omega}+\bar{d}_0(1-\xi^b)\right]^2 + \xi^{2a}} \tag{11b}$$

for the Gaussian and log-normal distribution, respectively. The RHS of these expressions is the sought-after resulting line shape. The difference of its half-width from unity and its shift are, respectively, the extra width and shift (in units of w_0) that the spectral line acquires due to the density distribution, whereas its area is the spectrally integrated intensity (in units of J_0). The total (spectrally integrated) line intensity can be factored out, leaving the normalized line shape

$$L_\tau(a,b,c,\sigma,\bar{d}_0;\bar{\omega}) = I(\bar{\omega})/J_\tau(c,\sigma), \tag{12}$$

where τ stands for the distribution type (G or LN) and

$$\frac{J_\tau(c,\sigma)}{J_0} = \frac{C_\tau(\sigma)}{\sigma\sqrt{2\pi}} \int_0^\infty d\xi \begin{cases} \xi^c \exp\left[-\frac{(\xi-1)^2}{2\sigma^2}\right] & ,\tau = G \\ \xi^{c-1}\exp\left[-\frac{(\ln\xi)^2}{2\sigma^2}\right] & ,\tau = \mathrm{LN} \end{cases} \tag{13}$$

($C_{\rm LN} \equiv 1$) with the small-σ parabolic asymptotes

$$J_\tau(c,\sigma)/J_0 \underset{\sigma\to 0}{=} \begin{cases} 1 + \frac{c(c-1)}{2}\sigma^2 & ,\tau = G \\ 1 + \frac{c^2}{2}\sigma^2 & ,\tau = \mathrm{LN}. \end{cases} \tag{14}$$

Evidently,

$$L_\tau(a,b,c,\sigma,-\bar{d}_0;\bar{\omega}) = L_\tau(a,b,c,\sigma,\bar{d}_0;-\bar{\omega}). \tag{15}$$

Contrary to the "unperturbed" Lorentzian shape in the absence of any density distribution, $L_\tau(a,b,c,\sigma,\bar{d}_0;\bar{\omega})$ is, in general, asymmetric. Therefore, it would be impossible to describe it by merely a width and a shift; instead, the widths and shifts at various fractions f ($0 \leq f \leq 1$) of the line-shape maximum can be used. Formally, let us define two positions at which the horizontal line at the fractional height f crosses the line shape as $\bar{w}_f^-$ and $\bar{w}_f^+$ (to the left and to the right of the peak, respectively):

$$L_\tau(\ldots;\bar{w}_f^\pm) = f \max_{\bar{\omega}\,\in\,\mathbb{R}} \{L_\tau(\ldots;\bar{\omega})\}. \tag{16}$$

Then, the fractional-height half-width and shift are [19]

$$\bar{w}_f = \frac{1}{2}(\bar{w}_f^+ - \bar{w}_f^-) \tag{17a}$$

and

$$\bar{d}_f = \frac{1}{2}(\bar{w}_f^+ + \bar{w}_f^-), \tag{17b}$$

respectively. Specifically, $f = 1/4$, $1/2$, $3/4$, and 1 (only the shift for the latter, evidently) will be used, see Fig. 1. Note that the fractional-height shift correction may even change its sign, as is seen in the figure (a slight negative shift of the line peak).

3. Results

In the impact limit (i.e., virtually for all isolated lines), $a = b = 1$. For hydrogen-like transitions, a varies from unity in the impact limit to $2/3$ when the quasistatic approximation [9] holds. A notable exception is the core of lines with a strong central Stark component, in particular, Lyman-α, attaining the so-called rotational broadening regime [18,20] with $a = 1/3$ in the high-density/low-temperature limit. In any case, each regime spans a large range of density so that a can be safely assumed constant on the scale of any reasonable σ. The Stark shift of hydrogen-like transition is exactly zero in the strict dipole approximation [21], arising only due to the quadratic Stark effect because of the state mixing with different principal quantum numbers and due

[1] Or its doubled value, full width at half-maximum (FWHM).

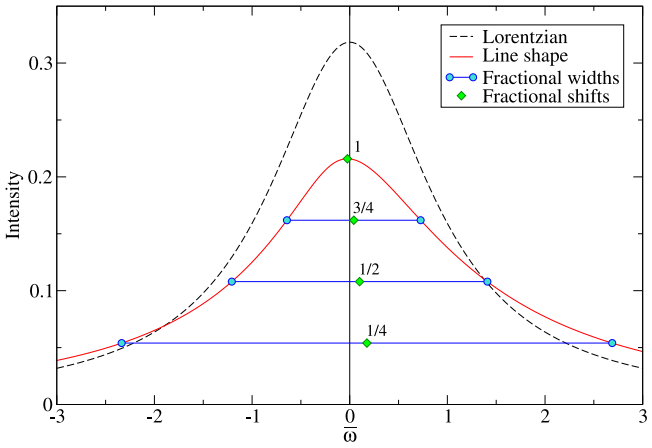

Fig. 1. Definition of widths and shifts at various fractions of the line-shape maximum. The area-normalized line shape shown corresponds to $a = b = 1$, $c = 2$, and $\bar{d}_0 = 0.25$. The log-normal density distribution with $\sigma = 0.5$ is assumed. For comparison, the "unperturbed" Lorentzian shape is also shown.

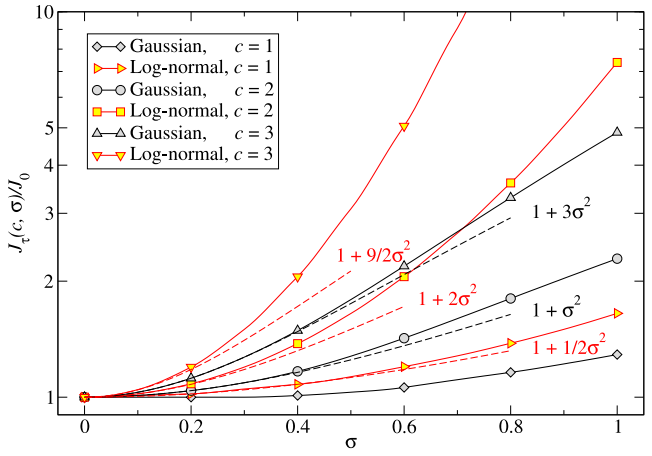

Fig. 2. $J_\tau(c,\sigma)/J_0$ for $c = 1$, 2, and 3. The $\sigma \to 0$ parabolic asymptotes are shown by the dashed lines.

to non-dipole interactions in the full-Coulomb-interaction models [22–24]. These effects result in nearly linear dependence of the shift on n_e (e.g., see [5,19]), i.e., $b \approx 1$. The line-intensity dependence on the density is typically quadratic—proportional to the number of emitting atoms and the number of electrons causing atomic level excitation per a plasma volume element, i.e., $c = 2$ (e.g., see Refs. [1,25]). However, if the plasma is close to the local thermodynamic equilibrium (LTE), the relative level populations become largely insensitive to the density, i.e., $c \approx 1$. Dipole-forbidden transitions may be more sensitive to n_e, however. Due to the Stark-effect induced mixing of atomic states with opposite parities, the radiative transition rate of such a transition, in the weak-field limit, depends on the second order of the plasma microfield magnitude, i.e., as $n_e^{4/3}$ [9]. Obviously, multiple concurring plasma-kinetics processes modify this dependence. To a good approximation, one extra power of the n_e-dependence can be assumed for forbidden lines, i.e., $c \approx 2$ and $c \approx 3$ for the LTE and non-LTE conditions, respectively. Self-absorption (opacity) may significantly reduce the sensitivity of the line intensity to the density, and furthermore, opacity deforms the line shapes. For these reasons, optically thick lines are rarely used for density diagnostics.

Based on the considerations above, five sets of the exponents $\{a, b, c\}$ are selected for the tabulations: $\{1,1,2\}$, $\{2/3,1,2\}$, $\{1,1,3\}$, $\{1,1,1\}$, and $\{2/3,1,1\}$. Variations of the line intensity $J_\tau(c,\sigma)/J_0$ as a function of σ are listed in Table 1 and shown in Fig. 2. Note the strong influence

Table 1
$J_\tau(c,\sigma)/J_0$ for $c = 1$, 2, and 3.

	Gaussian distribution			Log-normal distribution		
σ	$c=1$	$c=2$	$c=3$	$c=1$	$c=2$	$c=3$
0.1	1.00	1.01	1.03	1.01	1.02	1.05
0.2	1.00	1.04	1.12	1.02	1.08	1.20
0.3	1.00	1.09	1.27	1.05	1.20	1.50
0.4	1.01	1.17	1.49	1.08	1.38	2.05
0.5	1.03	1.28	1.79	1.13	1.65	3.08
0.6	1.06	1.42	2.19	1.20	2.05	5.05
0.7	1.11	1.60	2.69	1.28	2.66	9.07
0.8	1.16	1.80	3.29	1.38	3.60	17.81
0.9	1.22	2.03	4.02	1.50	5.05	38.28
1.0	1.29	2.29	4.86	1.65	7.39	90.02

of c on the line intensity. In particular, there is a significantly different effect for allowed ($c = 2$) and forbidden ($c = 3$) lines in a non-LTE plasma, especially in the case of the log-normal density distribution. In general, ratios of intensities of specific spectral line pairs (e.g., dielectronic satellites [26] or the inter-combination and resonance lines [27]) are often used for density diagnostics based on different sensitivity of the intensities of these lines to n_e. Evidently, even a moderate turbulence significantly impacts the density determination [3] based on measurements of line ratios (cf. a similar problem arising due to the *temperature* variations for plasma diagnostics based on T_e-sensitive line ratios [28]).

For convenience, relative deviations of the fractional-height widths and shifts from the respective "unperturbed" Lorentzian values ($\bar{w}_{0f}$ and $\bar{d}_0$) are reported,

$$\Delta\bar{w}_f \equiv \bar{w}_f/\bar{w}_{0f} - 1 \tag{18a}$$

$$\Delta\bar{d}_f \equiv \bar{d}_f/\bar{d}_0 - 1. \tag{18b}$$

Examples of the line-width and line-shift corrections for an isolated line ($a = b = 1$) are given in Fig. 3a and Fig. 3b, respectively. Notably, the corrections of the peak shift and of those at 3/4-height and below are of opposite signs (this can also be seen in Fig. 1). Furthermore, the peak-shift correction is a non-monotonous function of σ. Similar graphs, but for the quasistatic broadening ($a = 2/3$), are shown in Fig. 3c & d. In this case, the broadening is more homogeneous (that is, the extra widths at various heights are similar), and all shifts, including the peak shift, have the same sign. The case of an isolated dipole-forbidden transition is covered in Fig. 3e & f; it is qualitatively similar to the previous case. Contrary to that, the shape of an isolated line in an LTE plasma (panels g & h of the figure) is affected very differently: Here, the line becomes somewhat *narrower* in its upper half. There is also a significant decrease of the shift near the line peak, whereas the line pedestal is shifted in the opposite direction by a comparable value. Finally, a quasistatically broadened line under LTE conditions is considered in Fig. 3i & j.

Tables 2–6 cover the width and shift corrections for a few values of $\bar{d}_0$ from 0 to 1. Because of the symmetry relation (15), the tables are directly applicable also for negative ("red") shifts; indeed, a vast majority of spectral lines are red-shifted due to the Stark effect. If needed, the results can be interpolated over $\bar{d}_0$ (within each table) and over the a, b, and c exponents (between the tables). Evidently, in cases where such an interpolation is not applicable, Eqs. (11a) and (11b) can be used directly.

4. Discussion

4.1. Application to non-Lorentzian line shapes

From Eqs. (17) and (18) it follows that

$$\bar{w}_f^{\pm} = \bar{w}_{0f}^{\pm}(1 + \Delta\bar{w}_f) + \bar{d}_0(1 + \Delta\bar{d}_f). \tag{19}$$

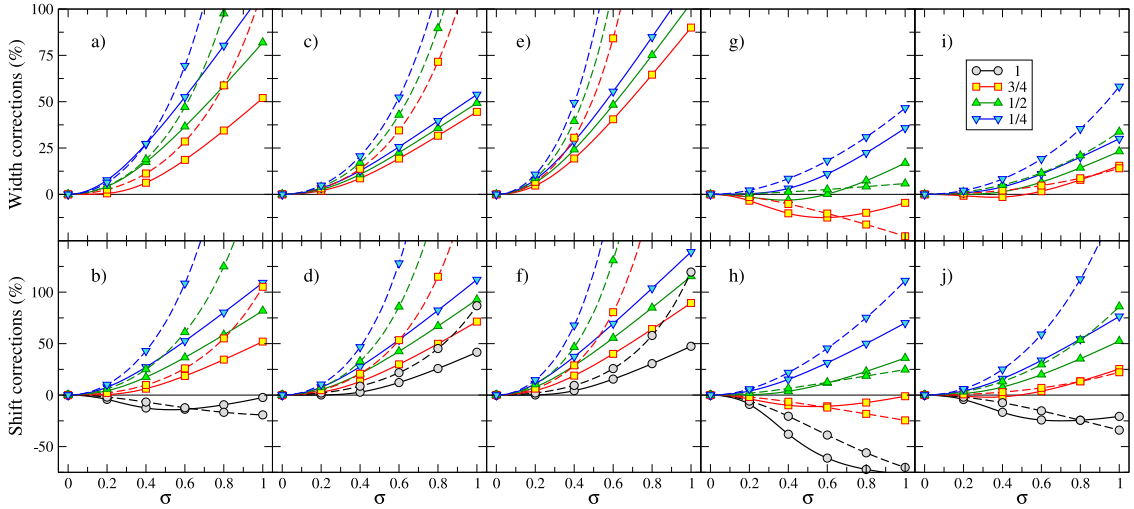

Fig. 3. Width (the upper panels) and shift (the lower panels) corrections at various fractional heights, as indicated in the legend. In columns from left to right: $a = b = 1$, $c = 2$; $a = 2/3$, $b = 1$, $c = 2$; $a = b = 1$, $c = 3$; $a = b = c = 1$; $a = 2/3$, $b = c = 1$. In all graphs, $\bar{d}_0 = 0.25$ with either Gaussian (solid lines) or log-normal (dashed lines) distribution assumed.

This expression can be used to apply the density-distribution corrections to non-Lorentzian line shapes, except that, instead of $\bar{w}_{0f} = \sqrt{1/f - 1}$ in the case of the Lorentzian shape, using appropriate analytical or numerical values.[2] In other words, the original line shape is non-linearly stretched according to Eq. (19). For arbitrary value of f, $\Delta\bar{w}_f$ and $\Delta\bar{d}_f$ can readily be obtained by inter- and extrapolation of values from Tables 2–6.

As a demonstration, consider a high-n Rydberg transition in the quasistatic limit. Its plasma-broadened shape is well described by the quasicontiguous (QC) approximation [29]. In an ideal plasma, it is given analytically by

$$L_{\mathrm{QC}}(\beta) = \frac{1}{\pi}\int_0^\infty \cos(\beta x)\exp(-x^{3/2})dx, \tag{20}$$

where β is a dimensionless quantity proportional to $\omega - \omega_0$; the proportionality factor is irrelevant here. Let us further assume a moderate red shift (say, 10% of the line FWHM, i.e., $\bar{d}_0 = -0.2$) due to the quadratic Stark effect. Using the respective values from Table 3 and interpolating them with a spline, one obtains a line shape that is in an excellent agreement with the exact calculation based on Eq. (2), as shown in Fig. 4. Note that this approach is also applicable to line shapes with multiple peaks, e.g., the hydrogen Balmer-β line.

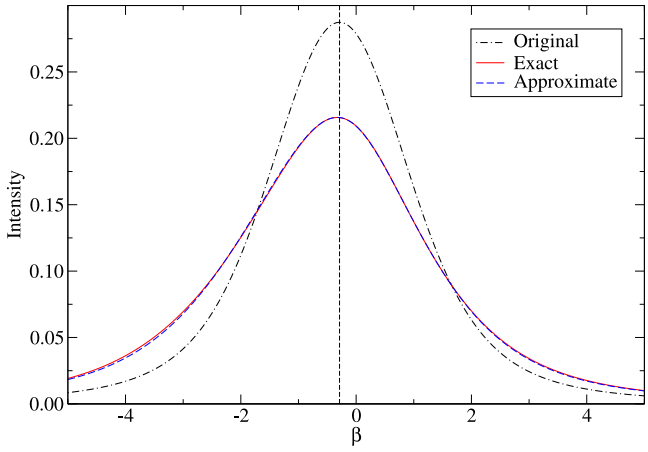

Fig. 4. An effect of the log-normal density distribution with $\sigma = 0.5$ on a hypothetical QC line shape with $\bar{d}_0 = -0.2$ assumed, labeled as "Original". $a = 2/3$, $b = 1$, and $c = 2$. The exact treatment according to Eq. (2) and the approximate one, based on the interpolated values from Table 3, are shown.

4.2. Minimizing uncertainties

A practical question can be asked: Which kind of spectral lines provides the most reliable density diagnostics if the density distribution is *not* known? Reviewing the results presented here (in particular, see Fig. 3), there appears to be no universal answer. It can be said, however, that the linear dependence of the line intensity or its absorption on the density, i.e., $c = 1$, results in the least uncertainty if the line width is used for the diagnostics. Within the $c = 1$ domain, the quasistatic-like width dependence ($a = 2/3$) ensures the least distorted shape, whereas the impact broadening ($a = 1$) gives the least sensitivity of FWHM. $c = 1$, however, implies an LTE plasma which may or may not be the case. The linear dependence on the density is typical for line absorption from the ground state of an atom even when the plasma is far from LTE. Thus, measurements of resonance-line absorption shapes are attractive in this respect, provided they are feasible (a backlighting source is present, etc.)

In the most common case ($c = 2$), however, there will unavoidably be a substantial increase of the line width and, therefore, an overestimation of the inferred n_e. At first sight, it may appear that the quasistatically broadened lines are preferable (cf. Fig. 3a and Fig. 3c), especially if the density distribution is Gaussian. When using such lines, however, the inferred density scales as $\propto w^{3/2}$, to be compared to $\propto w$ in the case of the isolated or otherwise linearly broadened lines. This stronger dependence largely negates smaller errors in the line width.

The answer is even less obvious in the case of line shifts. For all combinations considered, the shift corrections and their spread at different heights are roughly similar. Given the challenges of shift measurements in general (requirements of the absolute energy/wavelength calibration and, typically, smallness of the shift value compared to the line width) and larger theoretical uncertainties, this makes the density diagnostics based on line shifts even less reliable. There is, however, an interesting possibility of using a linear *combination* of line shifts at different fractional heights: For example, consider a dipole-allowed isolated line in a non-LTE plasma (Fig. 3b). In this case, an average value[3] of the shift

[2] If the initial shape is asymmetric, different $\bar{w}^-_{0f}$ and $\bar{w}^+_{0f}$ should be used for the left and right half-profiles, respectively.

[3] In these examples, "average" does not suggest exactly equal weights in the linear combinations; instead, they should be devised for a specific $\bar{d}_0$ based on Tables 2–6.

Table 2
Corrections (in %) to the fractional-height widths and shifts for $a = 1$, $b = 1$, $c = 2$, and various values of the reduced shift $\tilde{d}_0$.

	Gaussian distribution							Log-normal distribution						
σ	$\Delta\tilde{w}_{3/4}$	$\Delta\tilde{w}_{1/2}$	$\Delta\tilde{w}_{1/4}$	$\Delta\tilde{d}_1$	$\Delta\tilde{d}_{3/4}$	$\Delta\tilde{d}_{1/2}$	$\Delta\tilde{d}_{1/4}$	$\Delta\tilde{w}_{3/4}$	$\Delta\tilde{w}_{1/2}$	$\Delta\tilde{w}_{1/4}$	$\Delta\tilde{d}_1$	$\Delta\tilde{d}_{3/4}$	$\Delta\tilde{d}_{1/2}$	$\Delta\tilde{d}_{1/4}$
$\tilde{d}_0 = 0.0$														
0.1	0.01	0.51	1.00					0.50	1.01	1.51				
0.2	0.21	2.21	4.05					2.08	4.08	6.12				
0.3	1.20	5.46	9.15					4.88	9.42	14.15				
0.4	3.76	10.50	16.17					9.16	17.35	26.16				
0.5	8.01	17.14	24.73					15.24	28.40	43.07				
0.6	13.60	24.95	34.36					23.54	43.33	66.30				
0.7	20.14	33.58	44.73					34.60	63.23	97.95				
0.8	27.34	42.77	55.61					49.15	89.65	141.14				
0.9	35.00	52.36	66.84					68.19	124.79	200.43				
1.0	42.99	62.24	78.33					93.09	171.83	282.68				
$\tilde{d}_0 = 0.2$														
0.1	0.10	0.58	1.04	−1.01	0.03	1.02	1.98	0.59	1.07	1.55	−0.50	0.51	1.50	2.51
0.2	0.61	2.47	4.21	−4.23	0.51	4.24	7.67	2.40	4.32	6.29	−1.94	2.13	6.03	10.15
0.3	2.22	6.08	9.56	−9.37	2.38	9.79	16.37	5.63	9.96	14.54	−4.20	5.12	13.73	23.34
0.4	5.60	11.59	16.90	−13.99	6.19	17.36	27.19	10.52	18.34	26.90	−7.05	9.78	24.94	42.92
0.5	10.66	18.70	25.77	−16.45	11.69	26.41	39.38	17.42	30.01	44.32	−10.23	16.50	40.31	70.39
0.6	16.98	26.95	35.70	−16.87	18.42	36.46	52.46	26.78	45.79	68.30	−13.48	25.73	60.84	108.19
0.7	24.19	35.99	46.35	−15.80	25.99	47.19	66.12	39.19	66.85	101.04	−16.58	38.07	88.06	160.04
0.8	32.00	45.56	57.49	−13.72	34.13	58.39	80.17	55.47	94.84	145.80	−19.39	54.32	124.15	231.54
0.9	40.25	55.51	68.98	−10.94	42.69	69.91	94.51	76.71	132.15	207.39	−21.85	75.56	172.25	331.07
1.0	48.80	65.74	80.72	−7.67	51.54	81.67	109.04	104.46	182.18	293.01	−23.87	103.35	236.91	471.32
$\tilde{d}_0 = 0.4$														
0.1	0.35	0.76	1.16	−1.00	0.03	1.02	1.98	0.83	1.24	1.67	−0.49	0.51	1.50	2.51
0.2	1.74	3.22	4.70	−3.84	0.55	4.24	7.68	3.37	5.03	6.78	−1.83	2.15	6.04	10.17
0.3	4.91	7.73	10.64	−7.17	2.51	9.84	16.41	7.81	11.55	15.68	−3.69	5.19	13.77	23.40
0.4	10.03	14.26	18.65	−8.91	6.49	17.52	27.29	14.40	21.18	29.02	−5.63	10.01	25.11	43.11
0.5	16.72	22.35	28.19	−8.55	12.23	26.71	39.57	23.50	34.54	47.86	−7.31	17.06	40.76	70.88
0.6	24.52	31.51	38.74	−6.53	19.21	36.92	52.74	35.63	52.58	73.85	−8.46	26.88	61.86	109.26
0.7	33.09	41.40	49.98	−3.33	27.04	47.81	66.50	51.51	76.65	109.45	−8.93	40.15	90.05	162.18
0.8	42.20	51.78	61.69	0.67	35.45	59.16	80.65	72.18	108.74	158.31	−8.63	57.79	127.70	235.53
0.9	51.68	62.53	73.72	5.24	44.26	70.84	95.08	99.06	151.65	225.88	−7.47	81.07	178.24	338.19
1.0	61.43	73.52	86.00	10.20	53.35	82.76	109.71	134.16	209.47	320.32	−5.41	111.75	246.65	483.60
$\tilde{d}_0 = 0.6$														
0.1	0.77	1.06	1.36	−0.97	0.04	1.02	1.98	1.22	1.54	1.87	−0.48	0.51	1.50	2.51
0.2	3.54	4.42	5.49	−3.37	0.60	4.25	7.69	4.94	6.19	7.59	−1.67	2.17	6.04	10.19
0.3	8.87	10.22	12.26	−5.28	2.66	9.89	16.46	11.25	14.08	17.51	−3.02	5.30	13.83	23.49
0.4	16.30	18.09	21.15	−5.20	6.78	17.68	27.41	20.38	25.60	32.34	−3.99	10.33	25.32	43.38
0.5	25.10	27.43	31.53	−3.12	12.70	27.01	39.78	32.67	41.44	53.26	−4.22	17.77	41.34	71.54
0.6	34.81	37.75	42.87	0.45	19.90	37.37	53.06	48.77	62.73	82.15	−3.49	28.25	63.13	110.66
0.7	45.14	48.74	54.87	5.03	27.96	48.42	66.92	69.61	91.12	121.84	−1.67	42.57	92.47	164.90
0.8	55.91	60.18	67.30	10.32	36.59	59.93	81.17	96.55	129.04	176.59	1.40	61.78	131.97	240.53
0.9	66.99	71.95	80.05	16.09	45.62	71.77	95.71	131.57	179.99	252.72	5.84	87.37	185.42	347.01
1.0	78.31	83.95	93.01	22.22	54.93	83.84	110.44	177.39	249.05	359.82	11.86	121.39	258.31	498.77
$\tilde{d}_0 = 0.8$														
0.1	1.34	1.48	1.64	−0.94	0.05	1.02	1.98	1.77	1.95	2.15	−0.46	0.51	1.50	2.51
0.2	5.89	6.02	6.53	−2.86	0.68	4.25	7.69	7.05	7.76	8.68	−1.47	2.20	6.05	10.21
0.3	13.75	13.41	14.31	−3.65	2.89	9.93	16.50	15.76	17.45	19.93	−2.29	5.44	13.89	23.61
0.4	23.80	22.84	24.23	−2.25	7.17	17.79	27.53	28.00	31.33	36.63	−2.36	10.70	25.55	43.70
0.5	35.05	33.63	35.56	1.05	13.23	27.24	39.99	44.19	50.22	60.10	−1.34	18.53	41.93	72.27
0.6	47.01	45.29	47.80	5.72	20.56	37.73	53.36	65.13	75.46	92.52	0.96	29.63	64.39	112.16
0.7	59.45	57.55	60.66	11.31	28.74	48.91	67.32	92.06	109.09	137.17	4.74	44.89	94.86	167.76
0.8	72.22	70.22	73.92	17.55	37.50	60.55	81.68	126.79	154.09	199.02	10.20	65.52	136.19	245.70
0.9	85.25	83.17	87.48	24.22	46.67	72.52	96.31	171.92	214.83	285.52	17.59	93.24	192.49	356.06
1.0	98.46	96.34	101.25	31.22	56.12	84.72	111.14	231.19	297.65	407.99	27.27	130.43	269.82	514.25
$\tilde{d}_0 = 1.0$														
0.1	2.07	2.01	1.99	−0.89	0.06	1.02	1.98	2.47	2.48	2.50	−0.44	0.52	1.50	2.52
0.2	8.68	7.99	7.81	−2.37	0.80	4.25	7.70	9.64	9.72	10.04	−1.26	2.24	6.06	10.24
0.3	19.16	17.19	16.73	−2.23	3.27	9.93	16.55	21.10	21.52	22.86	−1.58	5.60	13.94	23.73
0.4	31.72	28.40	27.76	0.17	7.89	17.83	27.64	36.83	38.14	41.71	−0.85	11.12	25.75	44.03
0.5	45.30	40.80	40.13	4.40	14.27	27.34	40.18	57.32	60.49	68.08	1.22	19.36	42.46	73.00
0.6	59.44	53.95	53.35	9.91	21.87	37.92	53.63	83.65	90.19	104.46	4.85	31.06	65.52	113.62
0.7	73.95	67.62	67.14	16.29	30.30	49.19	67.68	117.45	129.72	154.67	10.28	47.15	97.00	170.50
0.8	88.74	81.64	81.31	23.25	39.29	60.94	82.12	161.16	182.73	224.47	17.78	68.99	139.96	250.59
0.9	103.72	95.92	95.76	30.63	48.67	73.00	96.85	218.18	254.55	322.58	27.75	98.45	198.84	364.56
1.0	118.85	110.39	110.40	38.31	58.33	85.30	111.77	293.39	353.02	462.32	40.71	138.23	280.22	528.75

Table 3
Same as Table 2 but for $a = 2/3$, $b = 1$, $c = 2$.

	Gaussian distribution							Log-normal distribution						
σ	$\Delta\tilde{w}_{3/4}$	$\Delta\tilde{w}_{1/2}$	$\Delta\tilde{w}_{1/4}$	$\Delta\tilde{d}_1$	$\Delta\tilde{d}_{3/4}$	$\Delta\tilde{d}_{1/2}$	$\Delta\tilde{d}_{1/4}$	$\Delta\tilde{w}_{3/4}$	$\Delta\tilde{w}_{1/2}$	$\Delta\tilde{w}_{1/4}$	$\Delta\tilde{d}_1$	$\Delta\tilde{d}_{3/4}$	$\Delta\tilde{d}_{1/2}$	$\Delta\tilde{d}_{1/4}$
$\tilde{d}_0 = 0.0$														
0.1	0.34	0.56	0.78					0.67	0.89	1.12				
0.2	1.42	2.28	3.09					2.71	3.62	4.53				
0.3	3.43	5.25	6.87					6.24	8.33	10.46				
0.4	6.58	9.42	11.86					11.45	15.29	19.26				
0.5	10.72	14.51	17.70					18.60	24.89	31.52				
0.6	15.54	20.17	24.04					28.10	37.72	48.07				
0.7	20.77	26.16	30.65					40.49	54.60	70.13				
0.8	26.24	32.31	37.37					56.48	76.66	99.43				
0.9	31.83	38.54	44.12					77.08	105.48	138.43				
1.0	37.47	44.77	50.84					103.65	143.30	190.67				
$\tilde{d}_0 = 0.2$														
0.1	0.42	0.62	0.82	0.00	0.68	1.34	1.98	0.75	0.95	1.16	0.50	1.17	1.85	2.52
0.2	1.76	2.52	3.25	0.07	2.88	5.37	7.71	3.05	3.87	4.71	2.03	4.79	7.53	10.39
0.3	4.22	5.77	7.20	0.55	6.99	12.01	16.55	7.03	8.93	10.89	4.67	11.14	17.56	24.52
0.4	7.93	10.28	12.42	2.37	13.12	20.80	27.65	12.95	16.45	20.13	8.56	20.75	32.82	46.65
0.5	12.64	15.71	18.50	5.93	20.89	31.12	40.20	21.18	26.92	33.10	13.93	34.43	54.81	79.61
0.6	18.02	21.73	25.07	10.95	29.80	42.45	53.69	32.26	41.09	50.83	21.13	53.37	85.85	127.91
0.7	23.80	28.06	31.91	17.05	39.49	54.45	67.78	46.98	60.00	74.81	30.65	79.34	129.47	198.70
0.8	29.82	34.56	38.86	23.90	49.71	66.92	82.29	66.41	85.22	107.24	43.19	114.93	191.05	303.19
0.9	35.95	41.14	45.85	31.29	60.31	79.70	97.07	92.13	118.96	151.38	59.72	163.96	278.80	459.32
1.0	42.14	47.73	52.82	39.07	71.17	92.71	112.06	126.40	164.51	212.15	81.62	232.11	405.42	695.88
$\tilde{d}_0 = 0.4$														
0.1	0.66	0.80	0.94	0.01	0.68	1.34	1.98	0.99	1.14	1.28	0.50	1.17	1.84	2.52
0.2	2.76	3.22	3.71	0.25	2.91	5.37	7.71	4.03	4.62	5.22	2.07	4.79	7.53	10.40
0.3	6.45	7.26	8.18	1.45	7.07	12.02	16.57	9.32	10.69	12.14	4.85	11.13	17.55	24.59
0.4	11.57	12.65	13.97	4.48	13.28	20.84	27.69	17.23	19.78	22.61	9.13	20.71	32.81	46.83
0.5	17.69	18.97	20.64	9.36	21.15	31.22	40.29	28.31	32.59	37.55	15.27	34.36	54.78	79.99
0.6	24.44	25.86	27.80	15.66	30.19	42.62	53.83	43.43	50.18	58.33	23.80	53.29	85.77	128.55
0.7	31.56	33.06	35.21	22.96	40.01	54.69	67.99	63.81	74.11	87.03	35.40	79.27	129.24	199.49
0.8	38.90	40.42	42.74	30.96	50.36	67.23	82.55	91.26	106.73	126.80	51.03	114.92	190.48	303.79
0.9	46.34	47.86	50.31	39.47	61.09	80.09	97.41	128.40	151.47	182.41	72.01	164.05	277.49	458.71
1.0	53.85	55.32	57.87	48.35	72.10	93.19	112.47	179.15	213.55	261.23	100.25	232.38	402.53	691.78
$\tilde{d}_0 = 0.6$														
0.1	1.07	1.10	1.13	0.03	0.69	1.34	1.98	1.39	1.44	1.48	0.51	1.17	1.85	2.53
0.2	4.37	4.36	4.46	0.50	2.95	5.37	7.72	5.63	5.83	6.06	2.12	4.78	7.53	10.42
0.3	9.86	9.58	9.69	2.42	7.21	12.03	16.59	12.93	13.47	14.14	5.11	11.10	17.54	24.68
0.4	16.95	16.26	16.32	6.44	13.53	20.88	27.75	23.73	24.90	26.46	9.81	20.67	32.77	47.08
0.5	25.00	23.83	23.81	12.31	21.52	31.30	40.40	38.78	41.01	44.18	16.69	34.29	54.68	80.45
0.6	33.59	31.94	31.77	19.54	30.68	42.75	54.00	59.26	63.22	69.09	26.33	53.19	85.55	129.19
0.7	42.50	40.34	39.99	27.72	40.64	54.89	68.22	86.93	93.65	103.92	39.50	79.16	128.82	200.20
0.8	51.59	48.89	48.31	36.55	51.14	67.49	82.86	124.37	135.52	152.83	57.29	114.81	189.69	304.23
0.9	60.76	57.51	56.68	45.86	62.03	80.41	97.79	175.45	193.64	222.25	81.22	163.99	276.08	458.22
1.0	69.99	66.16	65.03	55.53	73.20	93.57	112.93	245.91	275.36	322.24	113.48	232.43	400.12	689.16
$\tilde{d}_0 = 0.8$														
0.1	1.62	1.51	1.41	0.05	0.69	1.34	1.98	1.94	1.86	1.76	0.51	1.17	1.85	2.53
0.2	6.50	5.90	5.47	0.78	3.01	5.37	7.72	7.77	7.48	7.20	2.19	4.77	7.53	10.45
0.3	14.14	12.64	11.68	3.35	7.41	12.03	16.61	17.60	17.14	16.79	5.38	11.08	17.52	24.80
0.4	23.46	20.88	19.31	8.15	13.93	20.89	27.81	31.86	31.42	31.39	10.47	20.63	32.69	47.35
0.5	33.62	29.97	27.78	14.79	22.14	31.33	40.51	51.46	51.40	52.39	17.95	34.25	54.50	80.87
0.6	44.22	39.54	36.71	22.72	31.52	42.81	54.16	77.91	78.86	81.99	28.43	53.16	85.20	129.72
0.7	55.05	49.37	45.86	31.54	41.70	54.97	68.45	113.50	116.51	123.57	42.73	79.18	128.22	200.69
0.8	66.00	59.34	55.12	40.99	52.43	67.60	83.15	161.68	168.49	182.38	62.01	114.92	188.74	304.43
0.9	77.01	69.38	64.42	50.89	63.55	80.55	98.14	227.56	241.05	266.56	87.93	164.27	274.59	457.71
1.0	88.04	79.44	73.70	61.13	74.96	93.73	113.35	318.79	343.77	388.93	122.86	233.03	397.83	687.24
$\tilde{d}_0 = 1.0$														
0.1	2.33	2.03	1.75	0.08	0.70	1.34	1.98	2.65	2.39	2.12	0.52	1.17	1.84	2.53
0.2	9.08	7.81	6.72	1.08	3.10	5.37	7.72	10.40	9.53	8.62	2.27	4.77	7.52	10.49
0.3	19.05	16.31	14.06	4.20	7.69	12.01	16.63	23.12	21.54	19.99	5.64	11.07	17.48	24.93
0.4	30.65	26.35	22.84	9.64	14.46	20.85	27.85	41.14	39.02	37.15	11.07	20.62	32.58	47.59
0.5	42.96	37.16	32.40	16.86	22.93	31.27	40.59	65.54	63.21	61.71	19.03	34.27	54.25	81.21
0.6	55.58	48.38	42.39	25.32	32.57	42.74	54.30	98.15	96.26	96.29	30.14	53.26	84.76	130.09
0.7	68.36	59.83	52.59	34.64	42.99	54.90	68.63	141.85	141.53	144.94	45.26	79.40	127.52	200.97
0.8	81.21	71.39	62.88	44.55	53.97	67.51	83.38	200.93	204.10	214.02	65.62	115.35	187.66	304.43
0.9	94.08	83.01	73.20	54.89	65.33	80.45	98.42	281.77	291.70	313.43	92.94	165.02	273.00	457.13
1.0	106.95	94.65	83.52	65.55	76.98	93.61	113.67	393.93	416.22	458.79	129.75	234.27	395.53	685.60

Table 4
Same as Table 2 but for $a = 1$, $b = 1$, $c = 3$.

	Gaussian distribution							Log-normal distribution						
σ	$\Delta\tilde{w}_{3/4}$	$\Delta\tilde{w}_{1/2}$	$\Delta\tilde{w}_{1/4}$	$\Delta\tilde{d}_1$	$\Delta\tilde{d}_{3/4}$	$\Delta\tilde{d}_{1/2}$	$\Delta\tilde{d}_{1/4}$	$\Delta\tilde{w}_{3/4}$	$\Delta\tilde{w}_{1/2}$	$\Delta\tilde{w}_{1/4}$	$\Delta\tilde{d}_1$	$\Delta\tilde{d}_{3/4}$	$\Delta\tilde{d}_{1/2}$	$\Delta\tilde{d}_{1/4}$
$\tilde{d}_0 = 0.0$														
0.1	1.01	1.50	1.98					1.52	2.02	2.53				
0.2	4.17	6.01	7.73					6.24	8.33	10.46				
0.3	9.67	13.34	16.62					14.76	19.72	24.90				
0.4	17.34	22.92	27.79					28.10	37.71	48.05				
0.5	26.65	34.05	40.46					47.97	64.87	83.70				
0.6	37.05	46.19	54.07					77.07	105.44	138.36				
0.7	48.17	58.98	68.31					119.71	166.45	223.12				
0.8	59.79	72.22	82.95					182.87	259.66	357.31				
0.9	71.75	85.77	97.88					278.08	405.31	575.35				
1.0	83.95	99.54	113.01					424.86	638.91	940.24				
$\tilde{d}_0 = 0.2$														
0.1	1.09	1.56	2.02	0.01	1.03	2.00	2.94	1.60	2.08	2.57	0.50	1.52	2.52	3.54
0.2	4.52	6.25	7.88	0.12	4.41	7.88	11.12	6.58	8.58	10.63	2.06	6.30	10.36	14.65
0.3	10.46	13.84	16.95	0.99	10.47	17.07	23.06	15.58	20.32	25.33	4.83	15.02	24.44	34.95
0.4	18.66	23.72	28.32	3.60	18.87	28.58	37.31	29.70	38.87	48.91	9.08	28.83	46.62	67.71
0.5	28.47	35.15	41.19	8.07	28.90	41.55	52.93	50.77	66.94	85.32	15.26	49.59	80.16	118.78
0.6	39.35	47.58	55.00	13.94	39.98	55.43	69.38	81.71	108.97	141.24	24.01	80.22	130.54	198.40
0.7	50.93	60.65	69.42	20.77	51.74	69.91	86.36	127.20	172.35	228.17	36.15	125.38	206.97	324.47
0.8	62.98	74.16	84.24	28.25	63.97	84.78	103.68	194.84	269.52	366.15	52.83	192.66	325.09	528.76
0.9	75.36	87.97	99.35	36.19	76.52	99.92	121.25	297.23	421.86	590.99	75.65	294.65	511.99	869.02
1.0	87.98	101.99	114.66	44.46	89.30	115.26	139.00	455.77	667.06	968.32	106.86	452.75	815.83	1453.01
$\tilde{d}_0 = 0.4$														
0.1	1.34	1.74	2.14	0.02	1.03	2.00	2.94	1.84	2.26	2.69	0.51	1.52	2.52	3.54
0.2	5.55	6.94	8.33	0.42	4.44	7.89	11.13	7.59	9.32	11.14	2.18	6.32	10.37	14.66
0.3	12.69	15.25	17.87	2.31	10.56	17.10	23.08	17.96	22.05	26.58	5.38	15.10	24.49	35.02
0.4	22.15	25.89	29.75	6.42	19.05	28.66	37.37	34.25	42.20	51.41	10.74	29.10	46.81	67.94
0.5	33.16	38.05	43.10	12.41	29.19	41.70	53.03	58.58	72.75	89.86	19.01	50.31	80.74	119.41
0.6	45.17	51.16	57.38	19.70	40.39	55.66	69.53	94.40	118.69	149.18	31.20	81.86	132.00	199.94
0.7	57.82	64.90	72.25	27.85	52.28	70.21	86.55	147.31	188.35	241.88	48.65	128.77	210.22	327.96
0.8	70.91	79.05	87.51	36.57	64.63	85.15	103.93	226.53	295.86	389.88	73.27	199.25	331.83	536.32
0.9	84.30	93.49	103.05	45.70	77.30	100.37	121.55	347.46	465.68	632.56	107.96	307.04	525.46	885.00
1.0	97.90	108.13	118.78	55.12	90.20	115.79	139.34	536.50	741.22	1042.55	157.09	475.60	842.30	1486.40
$\tilde{d}_0 = 0.6$														
0.1	1.75	2.04	2.34	0.05	1.04	2.00	2.94	2.24	2.56	2.89	0.52	1.52	2.52	3.54
0.2	7.19	8.05	9.06	0.80	4.49	7.89	11.13	9.22	10.52	11.98	2.34	6.34	10.37	14.68
0.3	16.06	17.43	19.29	3.62	10.69	17.14	23.11	21.73	24.83	28.58	6.12	15.21	24.55	35.12
0.4	27.30	29.14	31.87	8.88	19.28	28.75	37.44	41.26	47.39	55.30	12.67	29.47	47.07	68.26
0.5	39.97	42.31	45.90	15.98	29.53	41.86	53.16	70.36	81.61	96.78	22.98	51.22	81.49	120.26
0.6	53.54	56.38	60.82	24.30	40.84	55.90	69.71	113.24	133.24	161.07	38.32	83.83	133.82	201.95
0.7	67.67	71.04	76.31	33.42	52.85	70.53	86.80	176.85	211.97	262.12	60.50	132.72	214.17	332.41
0.8	82.19	86.09	92.18	43.06	65.32	85.55	104.23	272.76	334.38	424.54	92.29	206.82	339.93	545.81
0.9	96.97	101.40	108.31	53.08	78.11	100.85	121.90	420.54	529.39	692.89	137.91	321.19	541.59	904.84
1.0	111.95	116.91	124.63	63.36	91.12	116.34	139.75	654.03	848.80	1149.93	204.06	501.80	873.99	1527.63
$\tilde{d}_0 = 0.8$														
0.1	2.32	2.45	2.61	0.08	1.05	2.00	2.94	2.80	2.98	3.17	0.54	1.52	2.52	3.54
0.2	9.36	9.54	10.04	1.21	4.56	7.90	11.14	11.42	12.16	13.12	2.55	6.37	10.38	14.71
0.3	20.32	20.26	21.13	4.85	10.88	17.16	23.15	26.66	28.51	31.23	6.91	15.37	24.61	35.25
0.4	33.64	33.29	34.57	11.03	19.60	28.82	37.52	50.21	54.12	60.33	14.58	29.90	47.33	68.63
0.5	48.26	47.68	49.40	18.98	29.97	41.99	53.29	85.14	92.89	105.58	26.67	52.20	82.25	121.20
0.6	63.66	62.91	65.09	28.10	41.41	56.09	69.90	136.69	151.49	175.95	44.71	85.81	135.62	204.10
0.7	79.56	78.68	81.32	37.96	53.53	70.79	87.04	213.50	241.30	287.14	70.97	136.50	218.08	337.07
0.8	95.78	94.81	97.91	48.33	66.11	85.88	104.53	330.10	381.88	467.09	108.99	213.91	347.93	555.62
0.9	112.23	111.19	114.76	59.04	79.01	101.25	122.27	511.26	607.70	766.61	164.33	334.39	557.48	925.17
1.0	128.85	127.75	131.78	70.00	92.14	116.81	140.17	800.27	980.92	1280.85	245.96	526.37	905.29	1569.71
$\tilde{d}_0 = 1.0$														
0.1	3.03	2.97	2.95	0.12	1.05	2.00	2.94	3.50	3.51	3.53	0.56	1.53	2.52	3.55
0.2	11.96	11.39	11.24	1.63	4.65	7.90	11.15	14.11	14.20	14.53	2.77	6.41	10.39	14.74
0.3	25.18	23.68	23.33	5.98	11.16	17.17	23.18	32.51	32.96	34.44	7.69	15.55	24.67	35.38
0.4	40.65	38.20	37.73	12.88	20.10	28.85	37.59	60.57	62.11	66.30	16.35	30.40	47.57	69.02
0.5	57.28	53.99	53.47	21.53	30.68	42.05	53.41	102.01	106.07	115.82	29.96	53.27	82.92	122.13
0.6	74.57	70.55	70.01	31.28	42.32	56.20	70.07	163.23	172.61	193.06	50.28	87.85	137.24	206.19
0.7	92.29	87.59	87.08	41.75	54.63	70.94	87.27	254.96	274.98	315.70	80.00	140.20	221.57	341.54
0.8	110.28	104.96	104.49	52.69	67.39	86.08	104.81	395.28	436.19	515.35	123.36	220.48	355.08	564.90
0.9	128.48	122.55	122.13	63.97	80.46	101.50	122.60	615.23	696.99	849.93	187.16	346.09	571.76	944.28
1.0	146.82	140.32	139.95	75.48	93.75	117.11	140.56	969.34	1131.44	1428.55	282.48	547.59	933.54	1609.12

corrections at the line peak and at 3/4 of its height stays very close to zero up to a moderate level of the density fluctuations. Alternatively, for the same line in an LTE plasma (Fig. 3h), an average of $\Delta\tilde{d}_{1/2}$ and $\Delta\tilde{d}_{3/4}$ can serve the same purpose.

4.3. Using line asymmetry to detect density distribution

It is possible to apply the results presented here to actually infer the density distribution. Indeed, if the "unperturbed" line shape is

Table 5
Same as Table 2 but for $a = 1$, $b = 1$, $c = 1$.

	Gaussian distribution							Log-normal distribution						
σ	$\Delta\tilde{w}_{3/4}$	$\Delta\tilde{w}_{1/2}$	$\Delta\tilde{w}_{1/4}$	$\Delta\tilde{d}_1$	$\Delta\tilde{d}_{3/4}$	$\Delta\tilde{d}_{1/2}$	$\Delta\tilde{d}_{1/4}$	$\Delta\tilde{w}_{3/4}$	$\Delta\tilde{w}_{1/2}$	$\Delta\tilde{w}_{1/4}$	$\Delta\tilde{d}_1$	$\Delta\tilde{d}_{3/4}$	$\Delta\tilde{d}_{1/2}$	$\Delta\tilde{d}_{1/4}$
$\tilde{d}_0 = 0.0$														
0.1	−1.01	−0.50						−0.50		0.50				
0.2	−4.12	−1.93	0.06					−1.92		1.96				
0.3	−9.35	−4.05	0.32					−4.15		4.33				
0.4	−15.21	−5.91	1.31					−6.98		7.50				
0.5	−19.55	−6.42	3.62					−10.25		11.42				
0.6	−21.80	−5.37	7.27					−13.81		16.02				
0.7	−22.35	−3.06	11.96					−17.54		21.27				
0.8	−21.70	0.15	17.40					−21.35		27.15				
0.9	−20.19	4.02	23.39					−25.18		33.65				
1.0	−18.10	8.36	29.77					−28.97		40.78				
$\tilde{d}_0 = 0.2$														
0.1	−0.92	−0.43	0.04	−2.06	−0.99	0.02	1.00	−0.42	0.06	0.54	−1.49	−0.49	0.49	1.49
0.2	−3.67	−1.64	0.25	−9.14	−3.74	0.30	3.98	−1.61	0.23	2.12	−5.78	−1.87	1.88	5.83
0.3	−7.77	−3.13	0.92	−23.62	−7.27	1.37	8.82	−3.46	0.50	4.68	−12.44	−3.93	3.94	12.72
0.4	−11.64	−3.88	2.66	−41.91	−10.08	3.60	15.21	−5.82	0.84	8.13	−20.79	−6.45	6.47	21.78
0.5	−14.14	−3.30	5.72	−57.71	−11.47	7.02	22.77	−8.55	1.25	12.40	−30.08	−9.27	9.27	32.70
0.6	−15.12	−1.43	9.95	−68.94	−11.47	11.43	31.19	−11.55	1.72	17.42	−39.62	−12.28	12.21	45.25
0.7	−14.78	1.49	15.08	−76.25	−10.34	16.62	40.22	−14.73	2.22	23.16	−48.87	−15.41	15.21	59.31
0.8	−13.45	5.21	20.90	−80.78	−8.35	22.40	49.70	−18.02	2.74	29.61	−57.49	−18.63	18.19	74.82
0.9	−11.37	9.53	27.22	−83.61	−5.71	28.63	59.52	−21.39	3.27	36.75	−65.16	−21.90	21.11	91.77
1.0	−8.74	14.28	33.92	−85.35	−2.58	35.21	69.60	−24.78	3.81	44.58	−71.94	−25.19	23.94	110.18
$\tilde{d}_0 = 0.4$														
0.1	−0.66	−0.25	0.17	−2.04	−0.98	0.02	1.00	−0.18	0.24	0.66	−1.48	−0.49	0.49	1.49
0.2	−2.39	−0.81	0.79	−8.57	−3.70	0.31	3.99	−0.68	0.91	2.60	−5.68	−1.86	1.88	5.85
0.3	−4.24	−1.03	2.29	−19.13	−7.06	1.47	8.89	−1.47	1.95	5.73	−11.98	−3.86	3.98	12.78
0.4	−5.24	−0.14	5.14	−30.15	−9.38	3.99	15.44	−2.52	3.26	9.95	−19.58	−6.25	6.61	21.95
0.5	−5.04	2.09	9.33	−39.11	−9.97	7.86	23.24	−3.82	4.78	15.15	−27.81	−8.83	9.63	33.08
0.6	−3.68	5.47	14.63	−45.58	−9.06	12.78	31.94	−5.38	6.45	21.29	−36.13	−11.48	12.93	46.00
0.7	−1.34	9.76	20.74	−49.97	−7.03	18.49	41.27	−7.18	8.22	28.31	−44.20	−14.14	16.43	60.62
0.8	1.75	14.71	27.45	−52.83	−4.21	24.79	51.05	−9.21	10.06	36.21	−51.81	−16.80	20.06	76.92
0.9	5.42	20.16	34.61	−54.59	−0.80	31.50	61.16	−11.45	11.95	44.97	−58.83	−19.45	23.78	94.93
1.0	9.52	25.99	42.09	−55.58	3.04	38.54	71.52	−13.86	13.85	54.63	−65.17	−22.10	27.53	114.70
$\tilde{d}_0 = 0.6$														
0.1	−0.24	0.06	0.37	−2.01	−0.98	0.02	1.00	0.22	0.53	0.86	−1.47	−0.49	0.49	1.49
0.2	−0.39	0.51	1.64	−7.95	−3.63	0.32	4.00	0.82	2.02	3.37	−5.52	−1.84	1.89	5.87
0.3	0.74	1.94	4.22	−16.12	−6.91	1.56	8.96	1.68	4.26	7.40	−11.36	−3.77	4.03	12.86
0.4	3.09	4.71	8.31	−23.66	−8.94	4.33	15.66	2.58	7.03	12.77	−18.18	−5.99	6.79	22.18
0.5	6.19	8.71	13.72	−29.28	−8.95	8.56	23.69	3.33	10.15	19.36	−25.40	−8.28	10.08	33.59
0.6	10.02	13.71	20.15	−32.99	−7.35	13.92	32.65	3.79	13.53	27.08	−32.67	−10.52	13.81	46.97
0.7	14.52	19.47	27.32	−35.16	−4.63	20.07	42.25	3.90	17.09	35.91	−39.75	−12.66	17.91	62.29
0.8	19.57	25.81	35.03	−36.20	−1.13	26.80	52.30	3.64	20.77	45.84	−46.53	−14.69	22.32	79.56
0.9	25.07	32.57	43.14	−36.40	2.91	33.94	62.67	3.01	24.56	56.91	−52.91	−16.65	26.97	98.86
1.0	30.92	39.65	51.55	−36.00	7.34	41.39	73.29	2.05	28.41	69.16	−58.84	−18.56	31.82	120.28
$\tilde{d}_0 = 0.8$														
0.1	0.35	0.49	0.65	−1.98	−0.97	0.02	1.00	0.76	0.94	1.13	−1.45	−0.49	0.49	1.49
0.2	2.19	2.25	2.78	−7.32	−3.53	0.33	4.01	2.85	3.54	4.42	−5.33	−1.81	1.89	5.89
0.3	6.63	5.65	6.59	−13.78	−6.61	1.62	9.03	5.79	7.34	9.61	−10.70	−3.64	4.08	12.97
0.4	12.87	10.45	12.00	−19.13	−8.59	4.56	15.87	9.07	11.91	16.43	−16.80	−5.67	6.98	22.45
0.5	19.63	16.31	18.66	−22.67	−8.63	9.08	24.09	12.30	16.99	24.69	−23.17	−7.69	10.54	34.16
0.6	26.46	22.98	26.25	−24.58	−6.83	14.76	33.26	15.21	22.41	34.32	−29.56	−9.56	14.69	48.02
0.7	33.26	30.29	34.52	−25.21	−3.63	21.26	43.09	17.66	28.09	45.30	−35.83	−11.24	19.38	64.04
0.8	40.27	38.08	43.27	−24.89	0.46	28.34	53.36	19.58	33.98	57.67	−41.89	−12.72	24.54	82.29
0.9	47.64	46.23	52.39	−23.88	5.05	35.82	63.97	20.97	40.05	71.50	−47.68	−14.03	30.12	102.88
1.0	55.36	54.65	61.77	−22.36	9.96	43.59	74.81	21.84	46.29	86.88	−53.18	−15.23	36.05	125.97
$\tilde{d}_0 = 1.0$														
0.1	1.10	1.03	1.01	−1.93	−0.96	0.02	1.00	1.45	1.46	1.48	−1.43	−0.48	0.49	1.50
0.2	5.22	4.38	4.15	−6.73	−3.39	0.32	4.02	5.34	5.42	5.73	−5.13	−1.77	1.90	5.92
0.3	12.77	10.00	9.33	−11.88	−6.02	1.61	9.09	10.68	11.06	12.29	−10.05	−3.49	4.13	13.08
0.4	22.12	17.01	16.11	−15.67	−7.37	4.63	16.05	16.60	17.71	20.76	−15.52	−5.31	7.16	22.73
0.5	31.94	24.81	24.05	−17.76	−6.92	9.34	24.42	22.52	24.99	30.90	−21.17	−7.04	10.95	34.73
0.6	41.80	33.22	32.83	−18.38	−4.90	15.28	33.77	28.13	32.69	42.65	−26.85	−8.56	15.48	49.04
0.7	51.66	42.12	42.21	−17.88	−1.71	22.05	43.79	33.22	40.73	56.01	−32.44	−9.85	20.69	65.71
0.8	61.59	51.41	52.02	−16.55	2.31	29.39	54.25	37.71	49.08	71.09	−37.89	−10.89	26.53	84.87
0.9	71.62	61.01	62.17	−14.60	6.91	37.13	65.05	41.54	57.72	87.99	−43.17	−11.72	32.94	106.66
1.0	81.77	70.85	72.55	−12.20	11.93	45.17	76.08	44.72	66.66	106.87	−48.23	−12.36	39.87	131.30

Table 6
Same as Table 2 but for $a = 2/3$, $b = 1$, $c = 1$.

	Gaussian distribution							Log-normal distribution						
σ	$\Delta\tilde{w}_{3/4}$	$\Delta\tilde{w}_{1/2}$	$\Delta\tilde{w}_{1/4}$	$\Delta\tilde{d}_1$	$\Delta\tilde{d}_{3/4}$	$\Delta\tilde{d}_{1/2}$	$\Delta\tilde{d}_{1/4}$	$\Delta\tilde{w}_{3/4}$	$\Delta\tilde{w}_{1/2}$	$\Delta\tilde{w}_{1/4}$	$\Delta\tilde{d}_1$	$\Delta\tilde{d}_{3/4}$	$\Delta\tilde{d}_{1/2}$	$\Delta\tilde{d}_{1/4}$
$\tilde{d}_0 = 0.0$														
0.1	−0.34	−0.11	0.11						0.22	0.44				
0.2	−1.36	−0.40	0.49					0.01	0.89	1.78				
0.3	−2.99	−0.68	1.29					0.05	2.02	4.02				
0.4	−4.43	−0.38	2.84					0.16	3.62	7.19				
0.5	−4.81	0.92	5.35					0.39	5.71	11.32				
0.6	−4.03	3.17	8.68					0.76	8.32	16.46				
0.7	−2.35	6.10	12.57					1.32	11.50	22.70				
0.8	−0.07	9.49	16.81					2.11	15.28	30.14				
0.9	2.62	13.17	21.28					3.17	19.71	38.91				
1.0	5.58	17.04	25.87					4.52	24.87	49.18				
$\tilde{d}_0 = 0.2$														
0.1	−0.25	−0.05	0.15	−1.02	−0.33	0.34	1.00	0.08	0.28	0.49	−0.50	0.17	0.83	1.50
0.2	−0.98	−0.14	0.66	−4.32	−1.18	1.51	4.03	0.33	1.13	1.95	−1.97	0.68	3.32	6.06
0.3	−1.96	−0.03	1.71	−10.56	−1.99	3.89	9.07	0.75	2.55	4.40	−4.35	1.58	7.44	13.80
0.4	−2.42	0.82	3.63	−18.13	−1.68	7.83	15.96	1.38	4.56	7.89	−7.52	2.90	13.18	24.96
0.5	−1.81	2.71	6.54	−24.03	0.24	13.24	24.28	2.24	7.17	12.46	−11.34	4.69	20.57	39.86
0.6	−0.15	5.49	10.22	−27.49	3.58	19.78	33.63	3.35	10.42	18.18	−15.67	7.00	29.67	58.97
0.7	2.30	8.91	14.44	−28.91	7.96	27.15	43.67	4.74	14.34	25.16	−20.37	9.87	40.59	82.92
0.8	5.30	12.76	19.01	−28.90	13.10	35.11	54.22	6.43	19.00	33.53	−25.29	13.32	53.50	112.54
0.9	8.67	16.89	23.78	−27.89	18.77	43.48	65.11	8.45	24.44	43.45	−30.33	17.40	68.63	148.89
1.0	12.30	21.19	28.68	−26.15	24.84	52.17	76.26	10.81	30.73	55.13	−35.39	22.15	86.26	193.30
$\tilde{d}_0 = 0.4$														
0.1	0.00	0.13	0.28	−1.01	−0.32	0.34	1.00	0.32	0.46	0.61	−0.50	0.17	0.83	1.50
0.2	0.11	0.62	1.16	−4.08	−1.15	1.51	4.03	1.26	1.84	2.43	−1.94	0.68	3.32	6.07
0.3	0.78	1.73	2.85	−8.81	−1.89	3.92	9.10	2.79	4.11	5.52	−4.18	1.56	7.44	13.86
0.4	2.43	3.82	5.58	−13.26	−1.42	7.94	16.05	4.86	7.26	9.91	−7.06	2.87	13.18	25.10
0.5	5.07	6.93	9.31	−15.93	0.77	13.51	24.47	7.42	11.28	15.68	−10.40	4.65	20.55	40.12
0.6	8.55	10.85	13.77	−16.67	4.42	20.24	33.94	10.44	16.18	22.93	−14.06	6.96	29.63	59.34
0.7	12.66	15.34	18.72	−15.88	9.14	27.82	44.12	13.89	22.00	31.79	−17.90	9.85	40.50	83.33
0.8	17.21	20.22	23.99	−13.97	14.61	35.98	54.80	17.75	28.78	42.44	−21.87	13.34	53.30	112.80
0.9	22.07	25.35	29.46	−11.24	20.61	44.57	65.83	22.01	36.59	55.09	−25.90	17.46	68.21	148.67
1.0	27.16	30.64	35.05	−7.91	27.01	53.47	77.13	26.67	45.52	70.02	−29.95	22.23	85.45	192.06
$\tilde{d}_0 = 0.6$														
0.1	0.41	0.44	0.48	−0.99	−0.32	0.34	1.00	0.71	0.76	0.81	−0.49	0.17	0.83	1.51
0.2	1.85	1.84	1.96	−3.76	−1.10	1.51	4.03	2.77	2.99	3.23	−1.88	0.67	3.32	6.09
0.3	4.85	4.41	4.58	−7.28	−1.74	3.93	9.13	6.00	6.59	7.30	−3.96	1.54	7.43	13.94
0.4	9.26	8.14	8.38	−9.83	−1.16	8.03	16.15	10.18	11.45	13.05	−6.52	2.83	13.15	25.30
0.5	14.50	12.82	13.14	−10.59	1.21	13.72	24.68	15.14	17.47	20.55	−9.38	4.60	20.49	40.45
0.6	20.30	18.20	18.58	−9.68	5.09	20.63	34.27	20.73	24.63	29.90	−12.43	6.90	29.52	59.76
0.7	26.51	24.07	24.47	−7.47	10.06	28.38	44.58	26.87	32.93	41.25	−15.60	9.79	40.31	83.73
0.8	33.05	30.26	30.65	−4.30	15.79	36.72	55.40	33.49	42.44	54.83	−18.85	13.30	53.00	113.03
0.9	39.84	36.67	37.00	−0.42	22.04	45.49	66.59	40.57	53.22	70.90	−22.15	17.46	67.75	148.48
1.0	46.80	43.23	43.47	3.98	28.68	54.56	78.03	48.09	65.39	89.83	−25.48	22.28	84.73	191.11
$\tilde{d}_0 = 0.8$														
0.1	0.97	0.86	0.75	−0.97	−0.31	0.34	1.00	1.26	1.17	1.08	−0.49	0.17	0.83	1.51
0.2	4.15	3.49	3.03	−3.42	−1.03	1.51	4.04	4.81	4.56	4.31	−1.82	0.67	3.31	6.12
0.3	9.77	7.86	6.80	−5.96	−1.45	3.92	9.15	10.18	9.87	9.66	−3.72	1.52	7.41	14.05
0.4	17.11	13.52	11.82	−7.18	−0.59	8.05	16.24	16.90	16.81	17.10	−5.98	2.80	13.09	25.51
0.5	25.20	20.01	17.75	−6.66	1.96	13.82	24.86	24.61	25.19	26.65	−8.43	4.56	20.38	40.76
0.6	33.63	27.05	24.29	−4.63	5.99	20.84	34.56	33.10	34.92	38.39	−11.02	6.86	29.33	60.12
0.7	42.27	34.47	31.23	−1.44	11.12	28.71	45.00	42.22	45.99	52.52	−13.69	9.75	40.04	84.05
0.8	51.07	42.16	38.43	2.60	17.01	37.18	55.94	51.89	58.49	69.30	−16.42	13.26	52.64	113.18
0.9	60.00	50.04	45.78	7.29	23.45	46.07	67.25	62.07	72.51	89.09	−19.20	17.44	67.27	148.32
1.0	69.04	58.04	53.23	12.45	30.28	55.26	78.82	72.73	88.20	112.34	−22.02	22.29	84.10	190.42
$\tilde{d}_0 = 1.0$														
0.1	1.69	1.39	1.11	−0.94	−0.31	0.34	1.00	1.95	1.70	1.44	−0.48	0.17	0.83	1.51
0.2	6.89	5.51	4.36	−3.07	−0.93	1.51	4.04	7.31	6.50	5.66	−1.75	0.66	3.31	6.15
0.3	15.23	11.98	9.43	−4.81	−1.04	3.88	9.17	15.13	13.81	12.52	−3.48	1.51	7.38	14.16
0.4	25.30	19.81	15.79	−5.05	0.26	7.96	16.30	24.61	23.09	21.86	−5.48	2.79	13.00	25.72
0.5	35.97	28.29	22.97	−3.61	3.23	13.75	25.00	35.25	34.03	33.63	−7.62	4.56	20.21	41.03
0.6	46.82	37.14	30.69	−0.78	7.60	20.82	34.80	46.74	46.49	47.92	−9.85	6.88	29.08	60.39
0.7	57.73	46.26	38.76	3.12	13.01	28.77	45.33	58.95	60.49	64.96	−12.14	9.79	39.71	84.26
0.8	68.69	55.58	47.04	7.81	19.17	37.30	56.38	71.77	76.11	85.08	−14.48	13.33	52.23	113.26
0.9	79.70	65.05	55.46	13.07	25.87	46.26	67.78	85.19	93.50	108.72	−16.87	17.52	66.76	148.15
1.0	90.75	74.62	63.97	18.78	32.96	55.51	79.45	99.17	112.85	136.45	−19.31	22.38	83.49	189.89

symmetric and the non-Stark broadening (e.g., due to the Doppler effect) can also be assumed symmetric, a presence of any asymmetry in the line shape can indicate a density distribution. The shifts and widths at different fractional heights then can be obtained and compared to the tabulated data [for the appropriate values of the line-shape density-dependence parameters, Eqs. (6)–(8) and (10)] to find a density distribution that gives the best match. Note that the absolute energy/wavelength calibration is not required, the relative shifts suffice. Evidently, the larger $\bar{d}_0$, the better accuracy is possible.

4.4. Units of measurements and "trivial" corrections

It is important to stress that all analytical expressions and tabulated values refer to line shapes expressed as a function of the angular frequency. The relative corrections remain unchanged if different, but proportional to the angular frequency, units are used, e.g., energy or wavenumber. However, wavelength units, that are still in wide use in plasma spectroscopy studies, would require a proper conversion except when the broadening, including the corrections in Tables 2–6, is exceptionally small compared to the unperturbed line wavelength. This is of particular importance for the accurate determination of line shifts.

Another potential caveat when modeling, or comparing to, experimental data, is a multiplicative factor, proportional to either ω^4 (if the spectral power is measured) or ω^3 (if the instrument records the photon numbers). Finally, the Boltzmann factor $\propto \exp(-\hbar\omega/kT)$ needs to be applied. Both of these non-linear corrections result in additional line asymmetry. Again, this is especially important for the line-shift-based analysis.

5. Conclusions

Any spectroscopy-based study of a plasma unavoidably collects light emitted from a finite plasma volume over a finite time determined by the spatial and temporal instrumental resolutions, respectively [2]. This results in spectroscopic features that are affected by a distribution of plasma parameters – notably, density and temperature – taking place during the time of observation. Indeed, most plasmas, in particular, unstable of turbulent ones, are characterized by non-uniformity of these parameters.

The present study analyzes effects of the density distribution on the shapes of discrete spectral lines often used for plasma density diagnostics [1]. It is shown that such a distribution distorts line shapes in a non-trivial way. Two distribution types, Gaussian and log-normal, are investigated over a wide range of the distribution variance. In the absence of a density distribution, the analysis assumes a Lorentzian line shape with its properties (the integrated intensity, width, and shift) dependent on the density via a small set of parameters [Eqs. (6)–(8)], allowing for application to different regimes of line broadening under various plasma conditions.

The results are presented analytically and also tabulated (Tables 2–6) in the form of line-width and line-shift corrections to ease their application in many cases. A way to apply these corrections to non-Lorentzian line shapes, avoiding brute-force evaluation by Eq. (2), is shown. This is of particular importance for line-shape modeling with high computational costs, such as computer simulations [30]. Provided also are considerations for choosing spectral lines to minimize uncertainties if a density distribution is expected but its extent is unknown. In addition, an approach for inferring the density distribution based on the line-shape asymmetry is suggested.

Throughout this paper, no influence of temperature variations has been considered. Obviously, temperature variations in the case of isothermal turbulence [11–13] are absent. In some other cases, a direct dependence (e.g., if the plasma evolution is adiabatic), or a statistical correlation between n_e and T, can be assumed. Under such conditions, the temperature dependences of the line width, shift, and intensity can be accounted for by modifying the respective exponents in Eqs. (6)–(8), at least as long as each of them can be approximated by a power law. Addressing more complex situations requires future work.

CRediT authorship contribution statement

Evgeny Stambulchik: Writing – review & editing, Writing – original draft, Visualization, Validation, Software, Methodology, Investigation, Conceptualization. **Yitzhak Maron:** Writing – review & editing, Validation, Project administration, Funding acquisition, Conceptualization.

Declaration of competing interest

The authors declare that they have no known competing financial interests or personal relationships that could have appeared to influence the work reported in this paper.

Data availability

Data will be made available on request.

Acknowledgments

This work was supported in part by the U.S.–Israel Binational Science Foundation (BSF), Israel and the Lawrence Livermore National Laboratory (USA).

References

[1] Griem HR. Principles of plasma spectroscopy. Cambridge, England: Cambridge University Press; 1997.
[2] Kunze H-J. Introduction to plasma spectroscopy. Springer series on atomic, optical, and plasma physics, vol. 56, Berlin, Heidelberg: Springer; 2009, http://dx.doi.org/10.1007/978-3-642-02233-3.
[3] Kroupp E, Stambulchik E, Starobinets A, Osin D, Fisher VI, Alumot D, et al. Turbulent stagnation in a Z-pinch plasma. Phys Rev E 2018;97:013202. http://dx.doi.org/10.1103/PhysRevE.97.013202.
[4] Rocco SVR, Lavine ES, Banasek JT, Potter WM, Hammer DA. Applying Thomson scattering to diagnosing turbulent density and velocity fluctuations in a gas-puff z-pinch. Phys. Plasmas 2022;29(11):110703. http://dx.doi.org/10.1063/5.0102312.
[5] Sobczuk F, Dzierzęga K, Stambulchik E. Plasma Stark effect of He II Paschen-α: Resolution of the disagreement between experiment and theory. Phys Rev E 2022;106(2):L023202. http://dx.doi.org/10.1103/PhysRevE.106.L023202.
[6] Maron Y, Doron R, Cvejić M, Stambulchik E, Mikitchuk D, Stollberg C, et al. Spectroscopic determination of magnetic fields in pulsed-power and high-energy-density plasmas. IEEE Trans Plasma Sci 2023;51(11):3407–25. http://dx.doi.org/10.1109/TPS.2023.3296561.
[7] Maron Y. Experimental determination of the thermal, turbulent, and rotational ion motion and magnetic field profiles in imploding plasmas. Phys. Plasmas 2020;27(6):060901. http://dx.doi.org/10.1063/5.0009432.
[8] Rosato J, Capes H, Marandet Y, Rosmej FB, Stamm R, Godbert-Mouret L, et al. Narrowing of Doppler spectral line shapes by correlated ion and electron temperature fluctuations. Europhys Lett 2008;84(4):43002. http://dx.doi.org/10.1209/0295-5075/84/43002.
[9] Griem HR. Spectral line broadening by plasmas. New York: Academic; 1974.
[10] Rosato J, Marandet Y, Peiffer A, Capes H, Godbert-Mouret L, Koubiti M, et al. Modeling of Stark-broadened lines in a fluctuating edge plasma. Contrib Plasma Phys 2014;54(4–6):565–9. http://dx.doi.org/10.1002/ctpp.201410045.
[11] Passot T, Vázquez-Semadeni E. Density probability distribution in one-dimensional polytropic gas dynamics. Phys Rev E 1998;58:4501–10. http://dx.doi.org/10.1103/PhysRevE.58.4501.
[12] Kritsuk AG, Norman ML, Padoan P, Wagner R. The statistics of supersonic isothermal turbulence. Astrophys J 2007;665(1):416. http://dx.doi.org/10.1086/519443.
[13] Hopkins PF. A model for (non-lognormal) density distributions in isothermal turbulence. Mon Not R Astron Soc 2013;430(3):1880. http://dx.doi.org/10.1093/mnras/stt010.
[14] Konjevic N, Lesage A, Fuhr JR, Wiese WL. Experimental Stark widths and shifts for spectral lines of neutral and ionized atoms (a critical review of selected data for the period 1989 through 2000). J Phys Chem Ref Data 2002;31(3):819–927. http://dx.doi.org/10.1063/1.1486456.
[15] Lesage A. Experimental Stark widths and shifts for spectral lines of neutral and ionized atoms: A critical review of selected data for the period 2001–2007. New Astron Rev 2009;52(11–12):471–535. http://dx.doi.org/10.1016/j.newar.2008.01.001.

[16] Stark-B – database for Stark broadening of isolated lines of atoms and ions in the impact approximation. https://stark-b.obspm.fr/.
[17] Rosato J, Capes H, Godbert-Mouret L, Koubiti M, Marandet Y, Stamm R. Accuracy of impact broadening models in low-density magnetized hydrogen plasmas. J Phys B: At Mol Opt Phys 2012;45(16):165701. http://dx.doi.org/10.1088/0953-4075/45/16/165701.
[18] Stambulchik E, Demura AV. Dynamic Stark broadening of Lyman-α. J Phys B: At Mol Opt Phys 2016;49(3):035701. http://dx.doi.org/10.1088/0953-4075/49/3/035701.
[19] Wiese WL, Kelleher DE, Paquette DR. Detailed study of the Stark broadening of Balmer lines in a high-density plasma. Phys Rev A 1972;6(3):1132–53. http://dx.doi.org/10.1103/PhysRevA.6.1132.
[20] Calisti A, Demura A, Gigosos MA, González-Herrero D, Iglesias CA, Lisitsa VS, et al. Influence of microfield directionality on line shapes. Atoms 2014;2(2):259–76. http://dx.doi.org/10.3390/atoms2020259.
[21] Alexiou S. On the pure dipole shift for hydrogen lines in a plasma. J Quant Spectrosc Radiat Transfer 2003;81:13–7. http://dx.doi.org/10.1016/S0022-4073(03)00048-7.
[22] Junkel GC, Gunderson MA, Hooper CF, Haynes DA. Full Coulomb calculation of Stark broadened spectra from multielectron ions: A focus on the dense plasma line shift. Phys Rev E 2000;62(4):5584–93. http://dx.doi.org/10.1103/PhysRevE.62.5584.
[23] Gomez TA, Nagayama T, Cho PB, Zammit MC, Fontes CJ, Kilcrease DP, et al. All-order full-Coulomb quantum spectral line-shape calculations. Phys Rev Lett 2021;127(23):235001. http://dx.doi.org/10.1103/PhysRevLett.127.235001.
[24] Stambulchik E, Iglesias CA. Full radiator-perturber interaction in computer simulations of hydrogenic spectral line broadening by plasmas. Phys Rev E 2022;105(5):055210. http://dx.doi.org/10.1103/PhysRevE.105.055210.
[25] Mihalas D. Stellar atmospheres. 2nd ed. W H Freeman & Co; 1978.
[26] Seely JF. Density-sensitive dielectronic satellite lines in microballon neon spectra. Phys Rev Lett 1979;42:1606–9. http://dx.doi.org/10.1103/PhysRevLett.42.1606.
[27] Doyle JG, Schwob JL. Intercombination to resonance line intensity ratio for He-like oxygen and carbon ions in TFR Tokamak plasmas. J Phys B: At Mol Opt Phys 1982;15(5):813. http://dx.doi.org/10.1088/0022-3700/15/5/023.
[28] McIntosh SW. On the inference of differential emission measures using diagnostic line ratios. Astrophys J 2000;533(2):1043–52. http://dx.doi.org/10.1086/308707.
[29] Stambulchik E, Maron Y. Stark effect of high-n hydrogen-like transitions: quasi-contiguous approximation. J Phys B: At Mol Opt Phys 2008;41(9):095703. http://dx.doi.org/10.1088/0953-4075/41/9/095703.
[30] Stambulchik E, Maron Y. Plasma line broadening and computer simulations: A mini-review. High Energy Density Phys 2010;6(1):9–14. http://dx.doi.org/10.1016/j.hedp.2009.07.001.